

Massive-Scale Dissolution, Conveyance, and Disposal of Dead Sea Potash Industry Halite Waste

Itay J. Reznik* and Ittai Gavrieli



Cite This: *Environ. Sci. Technol.* 2023, 57, 8385–8395



Read Online

ACCESS |

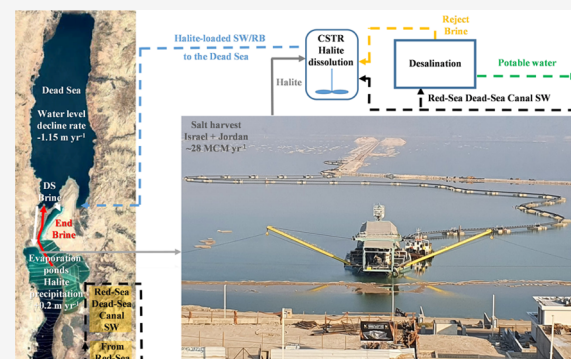
Metrics & More

Article Recommendations

Supporting Information

ABSTRACT: The Dead Sea (DS) potash industry halite waste accumulation rate is estimated at 0.2 m year^{-1} , across 140 km^2 of evaporation ponds in Israel and Jordan, totaling $\sim 28 \text{ million m}^3 \text{ year}^{-1}$. As accommodation in the southern DS basin space is nearly exhausted, it is planned in Israel to dredge newly precipitated salt and convey it in a solid state to the northern DS basin by constructing a 30 km conveyor to the northern DS basin where the salt will be disposed. Concerns regarding the environmental impacts of such massive undertaking led to the examination of alternative solutions. The alternative discussed in the paper, which takes into account the estimated halite waste volumes in Jordan as well, examines the feasibility for dissolution of the dredged halite and its transport in a dissolved state and disposal in the DS by seawater (SW) or desalination reject brine (RB) from the Red Sea—Dead Sea Project (RSDSP), if constructed. Results show that the high halite solubility in SW/RB and rapid dissolution kinetics are sufficiently fast to dispose of the dredged halite with the discussed volumes of the RSDSP. Thermodynamic calculations are presented to show that precipitation dynamics following the mixing of the $\text{Na}^+ - \text{Cl}^-$ -loaded SW/RB with the DS brine could be controlled to avoid outsalting at the mixing point in the DS.

KEYWORDS: Dead Sea, halite, Red-Sea Dead-Sea project, dissolution, submarine tailing disposal



1. INTRODUCTION

The Israel Chemicals Ltd (ICL) and the Arab Potash Company (APC) in the Hashemite Kingdom of Jordan extract potassium from the Dead Sea (DS) (Figure 1a) in order to supply a significant portion of the world fertilizer demands.¹ The industries operate independently, each pumping DS brine from the northern basin into evaporation ponds, which occupy an area of $\sim 250 \text{ km}^2$ ($\sim 140 \text{ km}^2$ in Israel; $\sim 110 \text{ km}^2$ in Jordan, Figure 1a). Initially, the brine evaporates to prompt the precipitation of halite, which has no commercial value (rock-waste). The brine is then transferred to an additional set of artificial ponds where the continuous evaporation and increased salinity prompt the precipitation of carnallite ($\text{KMgCl}_3 \cdot 6\text{H}_2\text{O}$). The latter is harvested and conveyed as sludge to the industrial plants for the production of commercial potash (KCl).² At the end of the process, the highly concentrated end brines (EBs) of both industries are discharged back to the DS through the Arava River.^{3,4}

The evaporation ponds are situated in the nowadays dry southern basin of the DS, at an elevation of -405 m . Prior to the 1980s, when the DS water-level was higher than $\sim -400 \text{ m}$ (Figure 1b), the northern and southern basins were connected. At the time, the area south of the Lisan peninsula had a water depth of few meters ($< 10 \text{ m}$).⁶ However, in the past 70 years, the DS natural water budget has been disrupted, mostly due to

anthropogenic activity such as upstream freshwater capture, as well as the enhancement of evaporation through increased surface area following the construction of the evaporation ponds. This led to a water-level decline of more than 45 meters since the 1950s. Recently, the rate of level decline has reached 1.15 m year^{-1} ,⁷ which is a manifestation of the $\sim 750 \text{ million cubic meters (MCM)}$ annual DS water deficit.

The negative DS water balance and the consequent salinity increase resulted in the early 1980s in the attainment of halite saturation and precipitation, which continues until today.^{8–10} Thus, currently both DS basins accumulate halite, and their bottom elevations rise. In the northern basin, uniform precipitation models calculate an average halite accumulation rate of 0.1 m year^{-1} .¹¹ Recent studies further showed that the halite deposits tend to chemically rework (seasonal dissolution/precipitation cycles) and concentrate below the thermocline, toward the center of the basin, leading to local accumulation rates of up to 0.25 m year^{-1} .^{9,12} This implies

Received: February 17, 2023

Revised: May 5, 2023

Accepted: May 8, 2023

Published: May 22, 2023



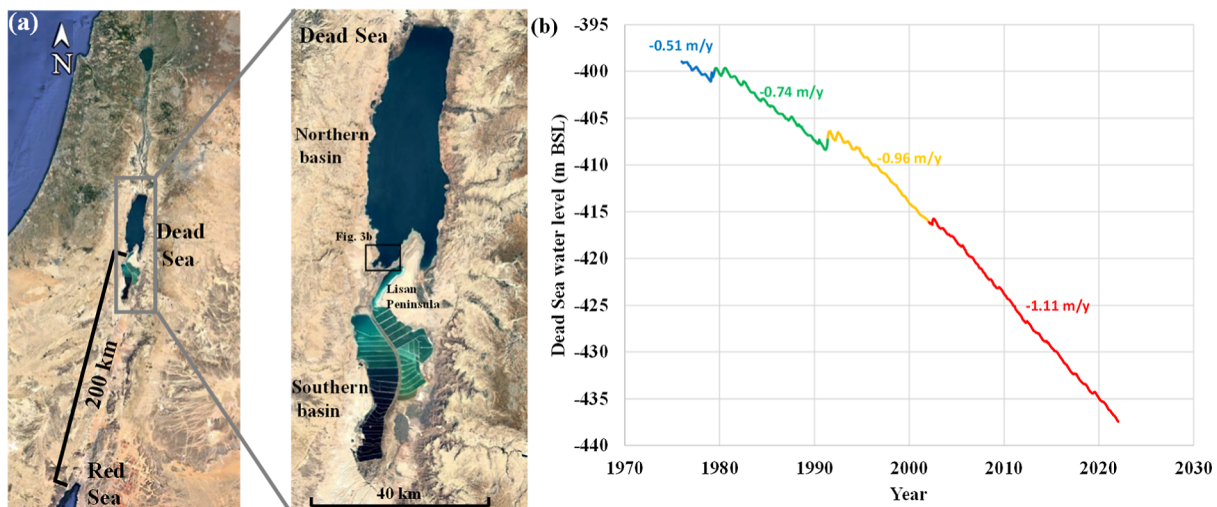


Figure 1. (a) Regional setting of the DS and the Red Sea with a close-up on the northern and southern DS basins. The southern basin hosts the potash plants' evaporation ponds. (b) DS water levels 1970–2022 (Hydrological-Service-of-Israel, 2022). Note the acceleration in the water level decline rate through the years.⁵



Figure 2. (a) Google Earth satellite view of the ICL salt piles. (b) Close-up view of the ICL salt piles. The picture faces west.

that since the 1980s, when halite first started precipitating, a salt layer of 4–10 m accumulated below the thermocline,¹² depending on the extent of the halite focusing mechanism.¹² Additional halite precipitation occurs locally where mixing between the highly concentrated EB and the DS brine takes place. This mixing results in instantaneous halite outsalting and precipitation, leading to the formation of a salt “delta” (see chapter 3.4) around the discharge point of the EB in the southern part of the northern DS basin.¹³

In the halite evaporation ponds, the rate of halite accumulation is estimated by ICL to be ~ 0.2 m year⁻¹. Based on this accumulation rate, it is estimated that since the beginning of operation, ~ 9 m of halite has accumulated in the halite evaporation ponds. In order to maintain a constant operative pond volume, the ICL had to raise the height of the embankments surrounding the ponds. The increasing pond base and water levels led to intrusion of the highly saline and corrosive brines into the coastal aquifer adjacent to the pond, risking the foundations of the surrounding structures, including one of Israel's largest hotel resorts. To mitigate this and to lower the water table of the aquifer, a series of pumping wells

have been installed which operate continuously. In addition, the Israeli planning committee issued a long-term regulatory framework, restricting the maximal level of the pond embankments to ~ 388.05 m¹⁴. Since this level has been reached, the equivalent volume of halite that precipitates has to be removed in order to maintain the pond operative volume. Given a pond area of 80 km² and an accumulation rate of 0.2 m year⁻¹, it follows that ICL has to dredge an annual waste salt volume of 16 MCM (equivalent to 35 million tons year⁻¹, assuming a salt density of 2.16 ton/m³). At the time of writing, the dredged salt is temporary dry stacked along the ICL halite evaporation pond. As of May 2023, the combined average dimensions of the mounds were $6600 \times 125 \times 15$ m (Figure 2).

The site selected in Israel for the eventual halite disposal of the halite is the northern basin of the DS (i.e., submarine tailings disposal), from which the salt was originally sourced from.¹⁴ Several nearshore underwater disposal sites have already been mapped¹⁵ and approved by Israel's Planning committee. Construction of a ~ 30 km long salt conveyor belt from the southern basin, across the Lynch strait to southern

shores of the northern basin, was also approved in principle. From there, the salt will be transported to sea either via ships or as slurry via pipelines. This suggested mega-operation includes either the construction of a port with constant traffic of ships and/or a large-scale heavy machinery industrial operations which will disrupt the unique and secluded environment of the DS. Additionally, these high-maintenance operations will have to be constantly adjusted to the ongoing receding DS level. Thus, the project as a whole will have a long-standing environmental footprint on the DS and its surroundings. In view of this, alternative solutions are being sought, e.g., the conveyance of the salt as suspended material in the EB channel around the discharge point to the DS.¹⁶ Here, we investigate the feasibility of dissolving, transporting, and disposing of the harvested halite by seawater (SW) or reject brine (RB) from desalination. The proposed solution will minimize much of the engineering undertaking described above, allowing to keep the required operation within the vicinity of the industrial areas nearby the evaporation ponds and is suited for both ICL and APC industries.

The proposed solution depends on the construction of the binational Red Sea—Dead Sea project (RSDSP), also known as the “Peace Conduit”, which was agreed upon in principle between Israel and Jordan. The RSDSP is a large-scale initiative aimed at changing the negative DS water balance by conveying SW from the Red Sea (~180 km), while also supplying SW for desalination to produce freshwater for a water scarce area. RB from desalination ($\times 1.8$ the salinity of SW) is to be conveyed to the DS, rather than to the Gulf of Eilat, which hosts a sensitive ecosystem. Furthermore, the elevation difference between the two seas will be used to generate hydroelectric power to cover some of the associated energy costs. The flux of SW and/or RB that will discharge into the DS will determine whether the rate of water-level decline will slow down, stabilize, or even rise. To date, however, the project did not come into fruition and was abandoned by the Jordanian and Israeli governments, primarily due to its high cost, environmental uncertainty, political setting, bureaucratic hurdles, and ongoing discussions regarding alternative projects.^{17–19} However, given the foreseen long-term water shortage in the region and the continuation of the DS water-level decline, the RSDSP is likely to be reconsidered in the near future. The additional proposed aspect of dissolving halite using the RSDSP may play a role in the decision-making process.

Through the years, numerous studies examined various expected effects of flowing SW/RB into the DS.²⁰ These effects include changes in limnological regime, gypsum precipitation,^{21–28} salinity and compositional changes,^{17,20,29} changes to evaporation rates, microbial blooming,³⁰ potential development of anoxic hypolimnion,²⁰ and sinkhole formation.³¹ The RSDSP feasibility study predicts that inflowing $<400 \text{ MCM year}^{-1}$ of either SW or RB will not alter the DS limnological state and will not lead to dilution of the surface waters. This will also prevent potential microbial blooming and possible “whitening”, which is the accumulation of gypsum at the DS surface water. Inflowing $<400 \text{ MCM year}^{-1}$ will allow to better examine the aforementioned effects, prior to the implementation of a full-scale project that aims to stabilize or even raise the lake level (~750/1000 MCM year⁻¹, respectively).²⁰

Halite dissolution has been vastly studied in natural processes, anthropogenic disrupted systems and industrial applications. These studies are used to better understand

salinity sources in sedimentary basins,^{32,33} dissolution of salt domes designated for radioactive waste disposal,³⁴ salt karsts,^{35,36} fluid inclusions,³⁷ subsurface halite dissolution during hydraulic fracturing,³⁸ drilling fluids makeup,³⁹ pressure solution,^{40,41} solution mining,⁴² and sinkhole formation.^{43,44} The dissolution kinetics was shown to be proportional to saturation state, available reactive surface area, mixing efficiency, temperature, salinity and the presence of catalysts/inhibitors. Halite dissolution was studied under a wide range of conditions, including natural and synthetic solutions, different salt morphologies (powder, thin plates, core samples), stirred/non-stirred batch, and flow-through experiments and under a temperature range of 25–80 °C.^{43–48} It was also reported that high concentrations ($>100 \text{ ppm}$) of some anions (I > Br > F) and metals (Cd > Pb > Cr > Co) in aqueous solutions lead to slower kinetics.^{45,49}

Despite the wide range of conditions tested, a general rate law for the dissolution of halite was not formulated. Furthermore, kinetic constants were found to range over ~ 2 orders of magnitude.^{43,45,47,49} Therefore, the ability to a-priori determine the reaction kinetics in SW/RB is limited and requires an experimental approach.

Consequently, the goals of the study is to examine whether SW/RB can dissolve the quantities required to dispose of the dredged halite. Furthermore, the study examines whether the dissolution kinetics are sufficiently fast to consider a large-scale dissolution plant that will be fed by SW/RB as part of the RSDSP operation. Lastly, the effect of re-precipitation of salt from the $\text{Na}^+ - \text{Cl}^-$ -loaded solutions upon mixing with the DS waters will be presented and discussed.

2. EXPERIMENTAL SECTION

2.1. Experimental Setup. Two sets of experiments were conducted using three experimental solutions: distilled water (DW), SW, and RB (Table S1) and samples of harvested salt:

- Thermodynamic experiments: 24 single-point batch experiments were performed to quantify the relationships between dissolved salts, electrical conductivity (EC), and density of the resulting solutions. For each solution, increasing quantities of halite were introduced (incremental increase of 50 g of NaCl per kg initial solution), until the added amount exceeded saturation. The derived data set was used to validate the accuracy of the Pitzer thermodynamic model (PhreeqC, USGS)^{50–53} by calculating and comparing the degree of saturation with respect to halite (DSH) at chemical equilibrium, as well as the dissolution and precipitation potentials (DPT and PPT, respectively). The experiments were conducted at room temperature (22.4–24.1 °C). The solutions were sampled and measured after 1 day and 1 week to verify that no further changes occurred.
- Kinetic experiments: six kinetic experiments were performed by instantaneously adding an excess amount (400 g/kg solution) of halite to beakers containing the three experimental solutions. To avoid diffusion-controlled kinetics, intensive magnetic stirring was used (300 rpm). Therefore, kinetics reported here are surface-controlled. The test matrix included also two sorted halite grain-size fractions from the harvested salt: 1.4–2 and 2–4 mm. Experiments were conducted at room temperature (23.6 to 24.1 °C). Experiments were

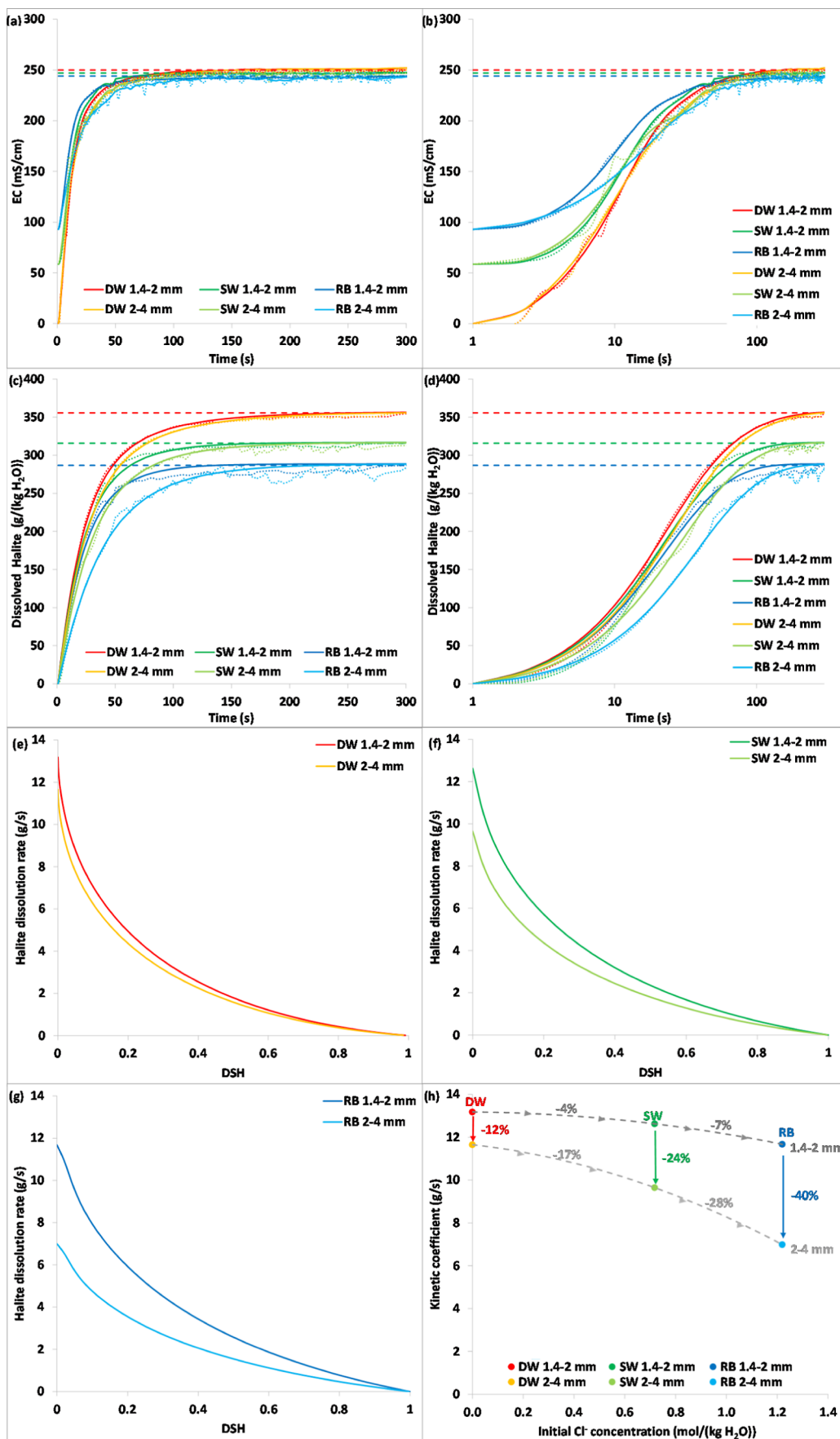


Figure 3. Results of the kinetic experiments: (a) EC as a function of time (s) (linear scale). Horizontal dashed lines represent the saturation values derived from the thermodynamic experiments. (b) Similar to subplot a, with time presented on a logarithmic scale. Solid lines in subplots a and b

Figure 3. continued

show the data following smoothing. (c) Dissolved halite ($\text{g NaCl/kg H}_2\text{O}$) as a function of time derived from the EC values (eq 1). (d) Similar to subplot c, with time presented on a logarithmic scale. (e–g) Halite dissolution rates (g/s) as a function of DSH for DW, SW, and RB, respectively. Solid lines in subplots c and d show the values calculated using eq 2. In each plot, the darker color represents the fine grain size fraction (1.4–2 mm), whereas the lighter color represents the coarse grain size fraction (2–4 mm). (h) Kinetic coefficients (eq 2) as a function of initial Cl^- concentrations. Note that with increasing salinity of the experimental solutions, the kinetic coefficients decrease, whereas the differences in the coefficients' values between the fine and coarse grain size fractions increase.

terminated after ~ 10 min once no change in EC was recorded.

2.2. Materials. SW was collected near the Mediterranean shore (Table S2). RB was collected from the Ashkelon desalination plant, Israel. RB is ~ 1.8 times more concentrated than the regular SW (Table S2). Note that the RB contains antiscalants, which are added to inhibit nucleation and growth of carbonate and sulfate minerals during desalination.

Halite was collected from ICL's harvested salt batteries 154/2 and 154/4 piled during 2021–2022. Samples were sieved to attain the two most frequently occurring particle-size fractions for the experiments (1.4–2 and 2–4 mm) with only 10% by mass of particles larger than 4 mm.

2.3. Analyses. Solution density was measured using DMA-35, Anton-Paar. EC and temperature were measured using WTW, 1970i at a 1 second frequency. Cations were analyzed by PerkinElmer Optima 3300 ICP–OES, and anions were analyzed by the Dionex Series 40001 gradient-ion-chromatograph, ($\pm 3\%$). Chloride concentrations were also analyzed by titration using 0.1 N AgNO_3 ($\pm 2\%$). Based on Ca^{2+} , K^+ , and Mg^{2+} analyses, X-ray diffraction, and scanning electron microscopy (SEM–EDS, FEI Quanta 450), only minor amounts of CaCO_3 and carnallite impurities were present in the halite (<0.5%).

3. RESULTS AND DISCUSSION

Thermodynamic and kinetic experimental conditions, chemical analysis, and geochemical modeling results are listed in Tables S1 and S2. The charge balance error of the analyzed samples did not exceed $\pm 2\%$. SEM analysis showed that the morphology of the halite crystals remained cubic despite crushing, transport, and long-term storage under open-air conditions (Figure S1).

3.1. Thermodynamic Experiments. In order to quantify the effect of halite dissolution on the solution physio-chemical properties, 24 experiments were conducted to experimentally derive the change in density (kg/L), EC (mS/cm), and DSH as a function of dissolved NaCl [$\text{g}/(\text{kg H}_2\text{O})$] (Figure S2). Density and EC experimental results were compared to the PhreeqC model output, which was set to synthetically react with halite with each experimental solution until saturation was attained. Modeling results showed a high-quality fit to the measured density ($\pm 0.0035 \text{ g/cm}^3$) (Figure S2, Ia,b). However, EC calculated by the PhreeqC model using the diffusion coefficients of the solutes,⁵¹ deviated from the experimental data toward the most saline samples (Figure S2, Ic). Therefore, instead of using the geochemical model, the following formulation was used to empirically describe the change in EC as a function of dissolved NaCl (Figure S2, Id)

$$\text{EC}_t = \text{EC}_i + K_1 \cdot \arctan \left(\frac{\text{NaCl(aq)}}{K_2} \right) \quad (1)$$

where EC_t and EC_i are the EC of the solution following and prior the dissolution, respectively (mS/cm), and NaCl(aq) is the amount of dissolved salt [$\text{g}/(\text{kg H}_2\text{O})$]. Computed K_1 constants were 211, 162, and 130 mS/cm , and K_2 constants were 140, 136, and 126 $\text{g NaCl}/(\text{kg H}_2\text{O})$ for DW, SW, and RB, respectively.

The results demonstrate the excellent fit of eq 1 to the data (Figure S2, Ic,d) as well as the deviation from linearity at higher concentrations. Note that since the EC does not decrease with increasing salinities, as reported for even higher salinity solutions,⁵⁴ the EC can still be used to unequivocally determine the amount of dissolved halite. Also note that the EC values of the solutions at saturation decrease in the order of DW > SW > RB, whereas the salinity order is reversed.

DSH values increase exponentially with dissolved halite until saturation is reached (Figure S2, Ie). Accordingly, near-saturation, a relatively small change in dissolved NaCl leads to a large change in DSH. This also implies that there is a greater uncertainty in determining DSH near-saturation in comparison with far-from-saturation conditions. Calculated DPTs of halite based on PhreeqC in the tested solutions are 356, 316, and 287 [$\text{g}/(\text{kg H}_2\text{O})$] for DW, SW, and RB, respectively (Figure S2, If). These large differences in DPT stem from the pre-existing or initial concentrations of Na^+ and Cl^- in the unreacted solutions. Since the Na/Cl molar ratio in SW and RB is lower than 1 (0.86), the initial dissolved NaCl is limited by Na^+ and is 34 and 58 $\text{g}/(\text{kg H}_2\text{O})$, respectively. Summation of the pre-existing dissolved halite (initial NaCl) and the DPT (added NaCl) yields the total dissolved halite at saturation (total dissolved NaCl) for DW, SW, and RB [356, 350, and 345 $\text{g}/(\text{kg H}_2\text{O})$], respectively, which significantly reduces the differences between the solutions. Consequently, the usage of total dissolved NaCl instead of added NaCl significantly normalizes the differences in density, EC, and DSH of the various solutions (compare Figures S2, IIa–c and S2, Ib,d,f). Note that with increasing NaCl concentrations, the chemical composition become more similar as their compositions are increasingly dominated by Na^+ and Cl^- (Table S2). The remaining small differences in total dissolved NaCl reflect the effect of the background electrolytes on the Na^+ and Cl^- activity coefficients.⁸

3.2. Kinetic Experiments. Kinetics of halite dissolution were studied for the three experimental solutions with two halite grain sizes (1.4–2 and 2–4 mm). Despite DPT differences between the experimental solutions, a similar initial amount of salt was added to all the kinetic experiments (400 $\text{g}/(\text{kg initial solution})$), which allowed for the same mineral/water ratio and stirring dynamics during the onset of the experiments (Table S1).

Continuous (1 s resolution) EC measurements were used to track the dissolution process. EC measurements were converted to the amount of added NaCl [$\text{g}/(\text{kg H}_2\text{O})$] using eq 1, thereby enabling the calculation of DSH. Using the reaction rates, the mass of solids present in the experiments

(proportional to the available reactive surface area) and the DSH, a rate law was formulated to quantify the reaction rate and provide grounds for quantitative comparison between the experiments. **Figure 3** shows the experimental results before (dotted lines) and after smoothing analysis (solid lines). Saturation values attained from the thermodynamic experiments are presented as horizontal dashed lines. Dotted lines represent the raw EC, which contained some noise that was likely generated by the fringe-field-effect resulting from the presence of the suspended halite particles near the electrode.⁵⁵ While most of the solid-phase interferences should be observed at the reaction onset (more particles in the suspension), the rapid increase in EC masks this noise. Near-saturation however, the amplitude of the noise can be observed. Further, note that higher noise is observed as a function of particle mass and size fraction.

In order to quantify the rate of reaction, the following simplified empiric rate law was fitted to the data:

$$\text{rate} = k \cdot (1 - \Omega) \cdot \left(\frac{m_t}{m_0} \right)^n \quad (2)$$

where rate is the halite dissolution rate (g/s), k is the kinetic coefficient (g/s), Ω is the DSH, m_t is the mass of halite (g) at time t (s), m_0 is the initial halite mass (g) and n is a dimensionless geometric coefficient that depends on the crystal shape and the relative dissolution rate of its different surfaces, i.e., reactive surface area.

Equation 2 was best fitted to the kinetic data by numerically iterating k and n values for each experiment. Average n values for all the experiments was 1.12 ± 0.3 (1σ), which is different from the theoretical value of $2/3$ surface area to mass ratio of a cube (square-cube law). This suggests that the actual reactive surface area is larger than the total surface area. Taking into account the uncertainties associated with the crystal geometry, reactive surface area, and experimental data, n was set as 1. Note that the formulated simplified first-order rate law ($n = 1$) adequately fits all the experimental data ($R^2 \geq 0.986$) (solid lines in **Figure 3c,d**).

Using this rate law ($n = 1$), the kinetic coefficients (k) values were derived by numerical iterations (**Figure 3e–g** at $\Omega = 0$). **Figure 3h** shows the non-linear negative relationship between the kinetic coefficients, salinity, and particle sizes. These relationships are also interdependent as no further simple normalization between parameters could be made. Overall, despite the observed differences, the reaction rates are all considered very fast. Taking into account the errors associated with the thermodynamic calculations and those associated with near-saturation EC measurements, a cutoff of $\text{DSH} = 0.9$ was taken as the estimated time to attain near-saturation conditions. According to the formulated rate laws, all experiments attained near-saturation conditions ($\text{DSH} = 0.9$) within 2.5 min.

3.3. Implications. The proposed solution for the conveyance and disposal in the DS of the harvested salt depends on the implementation of the binational RSDSP. If proven feasible, the APC and ICL would have similar rights to use the SW/RB for halite dissolution and transport. Thus, the following quantitative evaluation considers a total of 60 million tons of halite from ICL and APC combined (35 and 25 million tons year⁻¹, respectively).

Two extreme cases are considered: (i) far-from-saturation, short residence times, maximal water flux, minimal salt

concentration, and relatively small dissolution facility. Assuming a maximal SW/RB inflow of 400 MCM year⁻¹, as suggested by the RSDSP feasibility study, the complete dissolution of the annual amount of harvested salt (60 million tons/400 MCM) requires dissolution of 0.15 ton/m³ (150 g/L). This translates to 153 and 154 g NaCl/(kg H₂O) with a DSH of 0.15 and 0.22 for SW and RB, respectively. The residence time required to dissolve such an amount, according to the reaction kinetics, is 31 s with particle sizes <4 mm. (ii) Near-saturation, longer residence times, minimal water flux, maximal salt concentrations, and relatively larger dissolution facility are also considered. Assuming attainment of saturation [316 and 287 g/(kg H₂O) which translate to 311 and 279 g/L of the initial SW/RB, respectively], the minimal volume of SW/RB required to fully dissolve the annual amount of harvested salt is 193 and 215 MCM year⁻¹, respectively, i.e., only ~50% of the maximal volume recommended by the RSDSP feasibility study as a first stage of the project. As discussed above, the residence time to attain the required near-saturation conditions (defined by DSH = 0.9) is less than 2.5 min.

A continuous spectrum between case A and B is shown in **Figure S3a**. The figure demonstrates that with increasing volumes of SW or RB, less halite needs to be dissolved per volume of solution to dissolve the entire annual amount of dredged halite, translating into shorter dissolution times (**Figure S3b**). Using these values, the volume of a continuously stirred tank reactor (CSTR), within which halite dissolution can take place, can be estimated as:

$$V = \bar{\tau} \cdot Q \quad (3)$$

where V is the dissolution tank volume (m³), $\bar{\tau}$ is the mean residence time (s) required to dissolve the halite based on the reaction kinetics, and Q is the inflow flux (m³/s) derived from the annual SW/RB discharge volume. Based on **eq 3**, the calculated CSTR volumes for case B are 1800/2000 m³ for SW/RB, respectively. Increasing the inflow to ~280 MCM year⁻¹ (instead of using the minimal volumes) will reduce CSTR volumes to 500 m³ or even less for case A (**Figure S3c**).

In practice, the CSTRs may not behave ideally because of numerous reasons (e.g., dead zones where mixing may be less efficient) and therefore multiple reactors are usually connected in series which reduces the overall reactor volume.⁵⁶ Thus, the volume of the reactors as calculated above should be considered only as a first-pass estimate framework for planning and up-scaling.

Additional factors could also be considered to further improve the dissolution efficiency and CSTR size, such as grounding the harvested halite to smaller particle sizes. Furthermore, disposal surplus fine-grounded halite in the suspension by advection may be possible as well, provided sufficiently high flow rates.

3.4. Mixing Na⁺–Cl⁻-Loaded Solutions with DS Brine.

Following halite dissolution, Na⁺–Cl⁻-loaded solutions will be channeled to the northern DS basin where the solution will mix with the DS brine. This inflow is expected to change current halite precipitation dynamics due to change in the lake water balance as well as compositional differences between the water types. Particularly interesting is the potential for attainment of supersaturation upon mixing of the two brines, which will result in immediate and local salt precipitation (outsalting). This process is similar in nature to that occurring today in the vicinity of the outlet of the EB to the DS, where

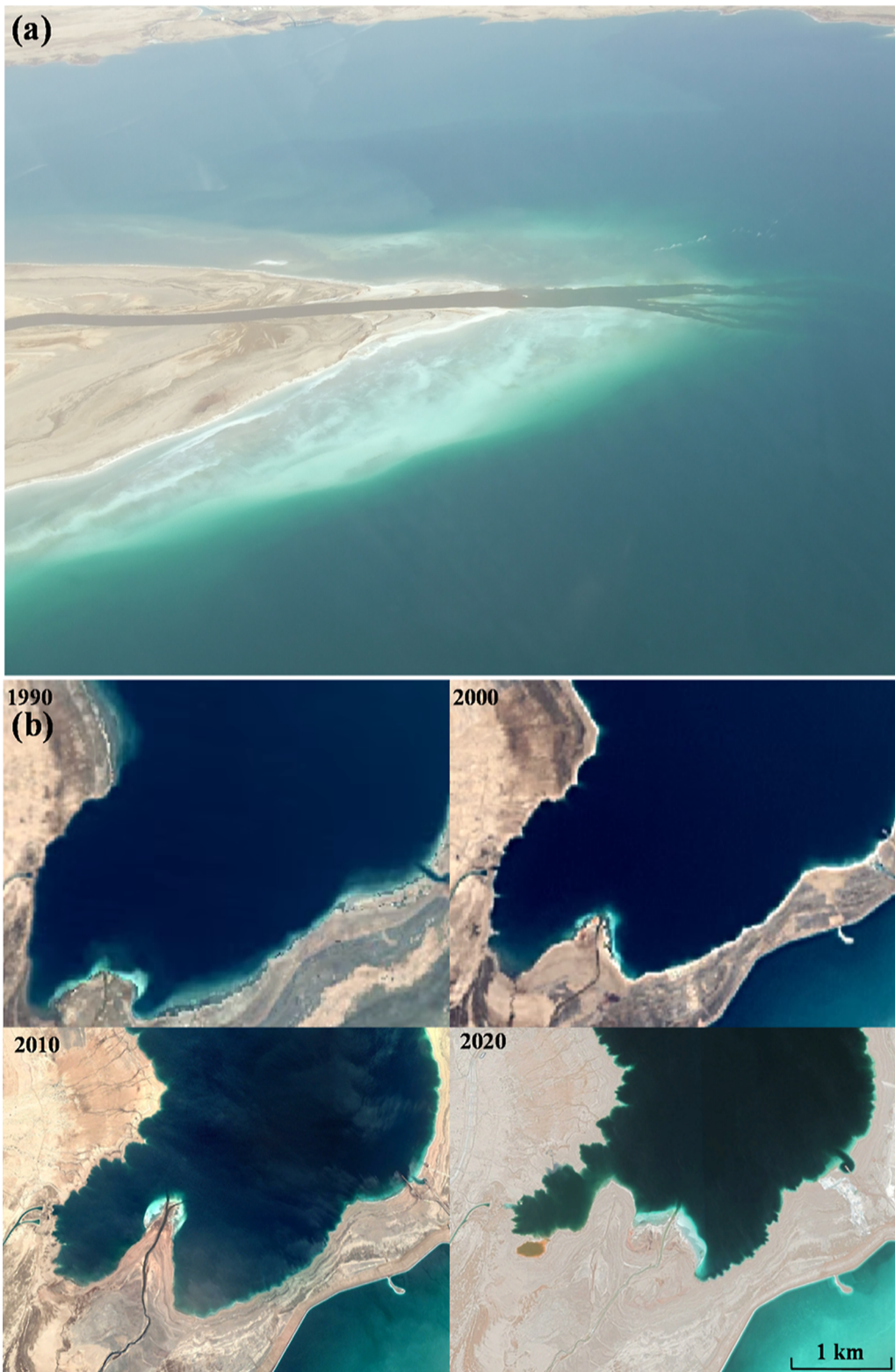


Figure 4. (a) Salt delta formed by chemical out salting at the outlet of the EB channel to the DS (photograph taken in 2009). (b) Set of Google Earth satellite images showing the progradation of the salt delta as well as the water level decline over time (1990–2020 at 10 year intervals).

the two halite-saturated brines mix. The resulting super-saturating and salt precipitation led over the decades to the formation and growth of the salt delta in the southern shores of the northern DS basin. Over the past decades, this process resulted in massive halite precipitation, which accumulated at the outlet mouth of the EB channel (Figure 4).

In order to examine the expected effect of mixing $\text{Na}^+ - \text{Cl}^-$ -loaded SW/RB solutions with the DS brine, chemical simulations were performed using the Pitzer model for the following extreme cases (Figure 5): case A (far-from-saturation) and B (saturation), as described above. For

reference purposes, case C was added to represent EB–DS mixing.

The results indicate that mixing either SW/RB halite-saturated solutions (case B) or EB (case C) with DS brine lead to the development of supersaturated solutions at all mixing ratios (**Figure 5a**). This is a manifestation of the lower halite solubilities in the resulting mixtures, which results in a positive PPT (**Figure 5b,c**). Thus, outsalting, salt precipitation, and formation of a salt delta may be expected under case B scenario. Interestingly, despite the fact that EB is Na^+ -depleted (case C), the PPT of EB–DS mixtures is higher than the PPT of halite-saturated SW/RB-DS mixtures (case B) (**Figure 5b**). Note that the rate of formation of the salt delta will depend on the discharged volumes in addition to the inflowing solution composition. It should also be noted that the potential retardation effect of the antiscalants that will be present in the RB on the halite outsalting kinetics has not been studied and may also affect the rate of salt delta formation. Lastly, the rate of halite outsalting at the salt delta will also depend on the mixing regime adjacent to the discharge point.

A completely different scenario is expected when mixing solutions from case A with DS brine. In this case, supersaturation does not occur, and thus no outsalting/salt delta formation is expected (**Figure 5a**). The fact that the salt delta formation can be avoided is a major environmental advantage of the proposed solution (case A) as a significant disruption to the unique natural DS landscape can be prevented. The 400 MCM year⁻¹ of the partially loaded SW/RB solutions will thus mix in the bulk DS, diluting the brine on the one end yet enriching it with Na^+ on the other (**Figure 5c**). The net result will be continuous halite precipitation throughout the lake, similar to present day dynamics. The amount that will precipitate will be equivalent to the total dissolved NaCl (6–10 initial NaCl + 28 added NaCl MCM year⁻¹). This salt volume divided by the $\sim 600 \text{ km}^2$ DS floor area calculates to an average accumulation rate of 5.5–6.5 cm year⁻¹, which is somewhat lower than the current average rate of 10 cm year⁻¹.

In summary, the RSDSP project was originally intended to provide potable water to the region through desalination, while slowing down the rate of DS water-level decline. Though not currently implemented, in the long run, as the water demand in the region continues to increase and the lake level will continue to drop, the execution of the project is likely to be reconsidered. The study discussed the integration of the salt-harvest project with the potential RSDSP, with the aim of investigating the potential for rapid dissolution of large salt volumes by SW/RB, while taking into consideration the volume limitations of the RSDSP project. Feasibility was demonstrated based on thermodynamic calculations, laboratory experiments, and geochemical modeling, yet it still has to be demonstrated in an up-scaled facility.

Kinetic experiments demonstrated that halite dissolution is rapid and that near-saturation conditions could be reached in less than 2.5 min. Dissolution rates could also be further increased if finer grain sizes are used. The results therefore shows feasibility for an industrial-scaled CSTR plant which could be reduced in size if higher SW/RB volumes are to be used.

It was shown that the precipitation regime in the DS could be controlled by the inflowing amounts or concentrations of dissolved halite in solution. Discharge of halite-saturated solutions will result in local outsalting and formation of a salt delta, whereas partially Na^+-Cl^- -loaded solutions will have

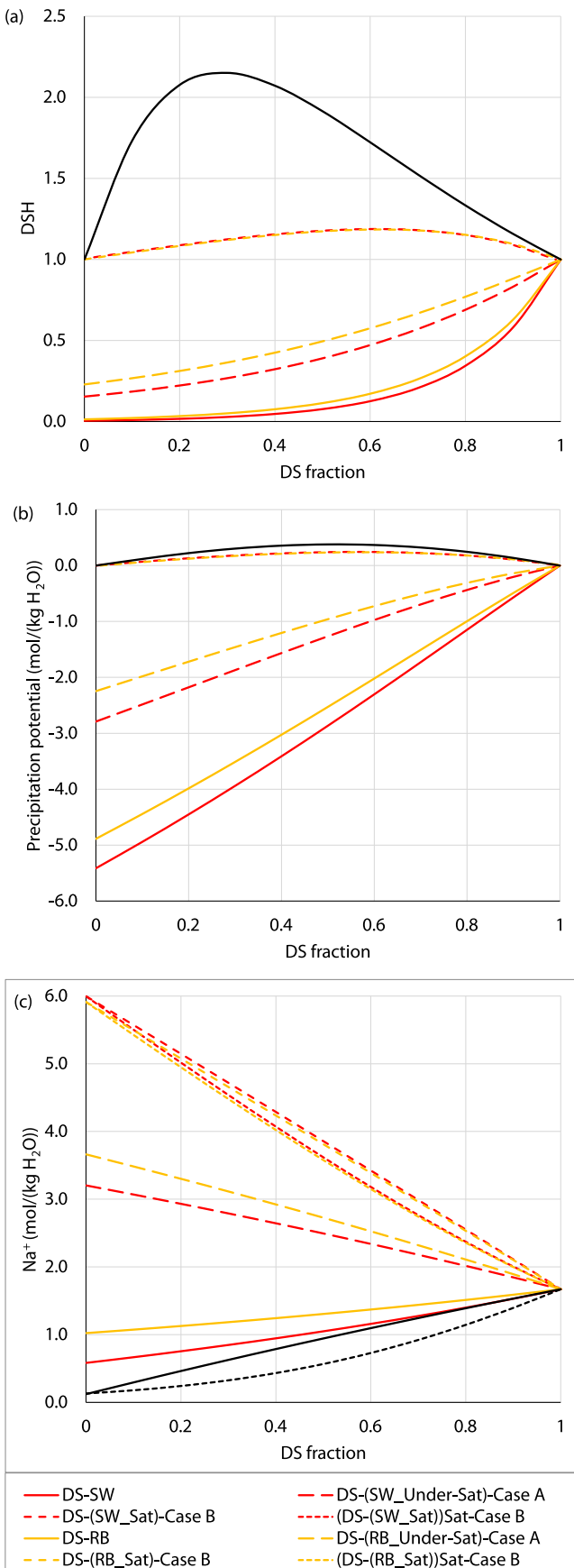


Figure 5. (a–c) Calculated DSH, PPT, and Na^+ concentrations for DS–SW, DS–RB, and DS–EB mixtures prior to any precipitation/dissolution; Under-Sat - Case A: mixtures between DS and far-from-

Figure 5. continued

saturation under-saturated SW/RB following limited halite dissolution; Sat - Case B: mixtures between DS and halite-saturated SW/RB following halite dissolution, denoted as "Sat" mixtures between DS and halite-saturated SW/RB. Mixtures following precipitation, denoted as (DS-(SW/RB_Sat))Sat; Case C:EB-DS mixtures. Halite saturated EB-DS mixtures following precipitation are denoted as (DS-EB)Sat.

no such effect. Rather, the added NaCl will precipitate throughout the lake as a result of evaporation and increased salinity, similar to present day dynamics.

By coupling and integrating the salt-harvest conveyance and disposal projects with the RSDSP, the environmental impact of the former could be minimized as the need to construct additional infrastructure for solid salt transport, and disposal could be bypassed. Furthermore, the solution offered here could prevent a scenario where the harvested salt will accumulate at the southern part of the northern DS basin, which could be the case if the salt will be transported and disposed of in a solid state. However, the feasibility and the environmental impacts of the RSDSP and the salt-harvest dissolution solution proposed here (both separately and coupled), remain to be evaluated and decided upon between the Israeli and Jordanian governments.

■ ASSOCIATED CONTENT

Supporting Information

The Supporting Information is available free of charge at <https://pubs.acs.org/doi/10.1021/acs.est.3c01197>.

SEM image of the harvested halite; thermodynamic experiments and results; salt concentrations, CSTR residence times and up-scaled plant volumes as function of SW/RB volumes; raw thermodynamic and kinetic experiments results; and chemical analysis of the thermodynamic and kinetic experiments ([PDF](#))

■ AUTHOR INFORMATION

Corresponding Author

Itay J. Reznik – Geological Survey of Israel, Jerusalem 9692100, Israel; orcid.org/0000-0002-1932-721X; Email: reznik@gsi.gov.il

Author

Ittai Gavrieli – Geological Survey of Israel, Jerusalem 9692100, Israel

Complete contact information is available at: <https://pubs.acs.org/10.1021/acs.est.3c01197>

Author Contributions

The manuscript was written through contributions of all authors. All authors have given approval to the final version of the manuscript.

Notes

The authors declare no competing financial interest.

■ ACKNOWLEDGMENTS

The authors thank the Israel Chemicals Ltd., (ICL) for supplying the harvested halite material and for the aerial photograph of the salt batteries. Specifically, we thank Eng. Shamaim Shriki for guiding us in the field and providing details

on the salt piles. We also thank Nayfa Sobeh who assisted in sieving the samples.

■ ABBREVIATIONS

APC	Arab Potash Company
CSTR	continuously stirred tank reactor
DPT	dissolution potential
DS	Dead Sea
DSH	degree of saturation with respect to halite
DW	distilled water
EB	end brines
ICL	Israel Chemicals Ltd
MCM	million cubic meters
PPT	precipitation potential
RB	reject brine
RSDSP	Red Sea—Dead Sea Project
SW	seawater

■ REFERENCES

- (1) Rabinowitz, G.; Mehrez, A. A multi-echelon multi-commodity, logistic system design at the Dead Sea Works Ltd. *Comput. Ind. Eng.* **2001**, *39*, 65–79.
- (2) García-Veigas, J.; Rosell, L.; Zak, I.; Playà, E.; Ayora, C.; Starinsky, A. Evidence of potash salt formation in the Pliocene Sedom Lagoon (Dead Sea Rift, Israel). *Chem. Geol.* **2009**, *265*, 499–511.
- (3) Nsour, M. F.; Al-Rjoub, S. A. Arab Potash Company (APC) Response Management Plan (RMP) to COVID-19. In *The Effect of Coronavirus Disease (COVID-19) on Business Intelligence*; Alshurideh, M. T., Hassani, A. E., Masa'deh, R. e., Eds.; Springer International Publishing: Cham, 2021;pp 289–310.
- (4) Epstein, J. A. Utilization of the dead sea minerals (a review). *Hydrometallurgy* **1976**, *2*, 1–10.
- (5) Lensky, N.; Dante, E. *The Causes of the Accelerated Drop of Dead Sea Level During the Last Decades (In Hebrew)*; GSI/16/2015; Geological Survey of Israel, 2015.
- (6) Lynch, W. *Narrative of the US Expedition to the River Jordan and the Dead Sea*; Rипол Классик: : London, 1849. R Bently
- (7) Hydrological-Service-of-Israel. *Dead Sea Water Level Elevation Dataset*; Jerusalem, 2022.
- (8) Gavrieli, I.; Starinsky, A.; Bein, A. The solubility of halite as a function of temperature in the highly saline Dead Sea brine system. *Limnol. Oceanogr.* **1989**, *34*, 1224–1234.
- (9) Sirota, I.; Arnon, A.; Lensky, N. G. Seasonal variations of halite saturation in the Dead Sea. *Water Resour. Res.* **2016**, *52*, 7151–7162.
- (10) Steinhorn, I. In situ salt precipitation at the Dead Sea. *Limnol. Oceanogr.* **1983**, *28*, 580–583.
- (11) Lensky, N. G.; Dvorkin, Y.; Lyakhovsky, V.; Gertman, I.; Gavrieli, I. Water, salt, and energy balances of the Dead Sea. *Water Resour. Res.* **2005**, *41*, W12418.
- (12) Sirota, I.; Enzel, Y.; Lensky, N. G. Halite focusing and amplification of salt layer thickness: From the Dead Sea to deep hypersaline basins. *Geology* **2018**, *46*, 851–854.
- (13) Beyth, M.; Katz, O.; Gavrieli, I. Progradation and retrogradation of the Salt Delta in the southern Dead Sea, 1985–1992. *Isr. J. Earth Sci.* **1997**, *46*, 95–106.
- (14) Israel-National-Infrastructure-Plan-35A, Dead Sea and Ancillary Protection Program—Long Term Solution—Salt Harvesting and Pumping Plan, National Planning Committee, 2016.
- (15) Lensky, N.; Gertman, I.; Rosentraub, Z.; Lensky, I.; Gavrieli, I.; Katz, O. *Alternative Dumping Sites in the Dead Sea for Harvested Salt from Pond 5*; Geological Survey of Israel: Jerusalem, Israel, 2010.
- (16) Lensky, N. G.; Ben Moshe, L.; Eyal, H.; Enzel, Y.; Calvo, R.; Vowinkel, B.; Aberle, J.; Meiburg, J.; Dante, E. Transport of Salt from the Salt Harvest via the Arava River. *Dead Sea Basin Infrastructure Response to Natural and Anthropogenic Changes: 2018–2028 Monitoring and Research Framework (In Hebrew)*; GSI/16/2022; Geological Survey of Israel: Jerusalem, 2022.

- (17) Closson, D.; Hansen, H.; Halgand, F.; Milisavljevic, N.; Hallot, F.; Achery, M. The Red Sea—Dead Sea Canal: Its Origin and the Challenges it Faces. In *Macro-engineering Seawater in Unique Environments: Arid Lowlands and Water Bodies Rehabilitation*; Badescu, V., Cathcart, R. B., Eds.; Springer Berlin Heidelberg: Berlin, Heidelberg, 2011; pp 107–124.
- (18) Asmar, B. N. The Science and Politics of the Dead Sea: Red Sea Canal or Pipeline. *J. Environ. Dev.* **2003**, *12*, 325–339.
- (19) Salem, H. The Red Sea—Dead Sea Conveyance (RSDSC) Project: A Solution for Some Problems or A Cause for Many Problems? In *Conference Proceedings of Water: Values and Rights, Ramallah, Palestine, April 13–15; United Nations Development Programme (UNDP), Programme of Assistance of the Palestinian People (PAPP), Palestinian Water Authority (PWA), and Palestine Academy for Science and Technology (PALAST)*; Ramallah: Palestine, 2009; pp 300–366.
- (20) Gavrieli, I.; Lensky, N.; Abelson, M.; Ganor, J.; Aharon, O.; Brenner, S.; Lensky, I.; Shalev, E.; Yechieli, Y.; Dvorkin, Y.; Gertman, I.; Scott, W.; Ehud, S.; Rosentraub, Z. *Red Sea—Dead Sea Water Conveyance Study Program—Dead Sea Study*; Springer, 2011.
- (21) Krunggalz, B. On the Problem of Gypsum Deposition in the Dead Sea in the Case of Two Seas Canal Construction. *Am. J. Phys. Chem.* **2019**, *8*, 58–65.
- (22) Reiss, A.; Gavrieli, I.; Rosenberg, Y.; Reznik, I.; Luttge, A.; Emmanuel, S.; Ganor, J. Gypsum Precipitation under Saline Conditions: Thermodynamics, Kinetics, Morphology, and Size Distribution. *Minerals* **2021**, *11*, 141.
- (23) Reiss, A. G.; Ganor, J.; Hamawi, M.; Gavrieli, I. Dynamics of turbidity in gypsum-precipitating brines: The case of the Red Sea—Dead Sea project. *J. Environ. Manage.* **2021**, *288*, 112369.
- (24) Reznik, I.; Ganor, J.; Gal, A.; Gavrieli, I. Gypsum saturation degrees and precipitation potentials from Dead Sea—seawater mixtures. *Environ. Chem.* **2009**, *6*, 416.
- (25) Reznik, I.; Ganor, J.; Gruber, C.; Gavrieli, I. Towards the establishment of a general rate law for gypsum nucleation. *Geochim. Cosmochim. Acta* **2012**, *85*, 75–87.
- (26) Reznik, I. J.; Ganor, J.; Lati, J.; Aharoni, M.; Cohen, O.; Maymon, M.; Gavrieli, I. Gypsum precipitation dynamics in a large experiment. In *Water-Rock Interaction—Proceedings of the 13th International Conference on Water-Rock Interaction, WRI-13*; CRC Press, 2010; pp 489–492.
- (27) Reznik, I. J.; Gavrieli, I.; Antler, G.; Ganor, J. Kinetics of gypsum crystal growth from high ionic strength solutions: a case study of Dead Sea—seawater mixtures. *Geochim. Cosmochim. Acta* **2011**, *75*, 2187–2199.
- (28) Reznik, I. J.; Gavrieli, I.; Ganor, J. Kinetics of gypsum nucleation and crystal growth from Dead Sea brine. *Geochim. Cosmochim. Acta* **2009**, *73*, 6218–6230.
- (29) Gavrieli, I.; Bein, A.; Oren, A. The expected impact of the “Peace Conduit” project (the Red Sea—Dead Sea pipeline) on the Dead Sea. *Mitig. Adapt. Strategies Global Change* **2005**, *10*, 3–22.
- (30) Oren, A.; Gavrieli, J.; Kohen, M.; Lati, J.; Aharoni, M.; Gavrieli, I. J. N. R.; Issues, E. Long-term mesocosm simulation of algal and archaeal blooms in the Dead Sea following dilution with Red Sea water. *Natural Resources and Environmental Issues* **2009**, *15*, 27.
- (31) Yechieli, Y.; Abelson, M.; Bein, A.; Crouvi, O.; Shtivelman, V. Sinkhole “swarms” along the Dead Sea coast: Reflection of disturbance of lake and adjacent groundwater systems. *Geol. Soc. Am. Bull.* **2006**, *118*, 1075–1087.
- (32) Chi, G.; Savard, M. M. Sources of basinal and Mississippi Valley-type mineralizing brines: mixing of evaporated seawater and halite-dissolution brine. *Chem. Geol.* **1997**, *143*, 121–125.
- (33) Hanor, J. S. Origin of saline fluids in sedimentary basins. *Geological Society, London, Special Publications* **1994**, *78*, 151–174.
- (34) Kloppmann, W.; Négrel, P.; Casanova, J.; Klinge, H.; Schelkes, K.; Guerrot, C. Halite dissolution derived brines in the vicinity of a Permian salt dome (N German Basin). Evidence from boron, strontium, oxygen, and hydrogen isotopes. *Geochim. Cosmochim. Acta* **2001**, *65*, 4087–4101.
- (35) Cooper, A. H. Halite karst geohazards (natural and man-made) in the United Kingdom. *Environ. Geol.* **2002**, *42*, 505–512.
- (36) Frumkin, A. Hydrology and denudation rates of halite karst. *J. Hydrol.* **1994**, *162*, 171–189.
- (37) Lazar, B.; Holland, H. D. The analysis of fluid inclusions in halite. *Geochim. Cosmochim. Acta* **1988**, *52*, 485–490.
- (38) Seales, M.; Dilmore, R. M.; Ertekin, T.; Wang, J. Y. Development of a halite dissolution numerical model for hydraulically fractured shale formations (Part I). *J. Unconv. Oil Gas Resour.* **2016**, *15*, 66–78.
- (39) Scheid, C. M.; de Carvalho, R. V.; de Oliveira, B. R.; de Oliveira Borges, R. F.; Calçada, L. A. Evaluation of the dissolution kinetics of NaCl particles in aqueous drilling fluids viscosified with bentonite. *J. Pet. Sci. Eng.* **2019**, *174*, 563–571.
- (40) Gratier, J.-P. Experimental pressure solution of Halite by an indenter technique. *Geophys. Res. Lett.* **1993**, *20*, 1647–1650.
- (41) Hickman, S. H.; Evans, B. Kinetics of pressure solution at halite-silica interfaces and intergranular clay films. *J. Geophys. Res.: Solid Earth* **1995**, *100*, 13113–13132.
- (42) Field, L.; Milodowski, A. E.; Evans, D.; Palumbo-Roe, B.; Hall, M. R.; Marriott, A. L.; Barlow, T.; Devez, A. Determining constraints imposed by salt fabrics on the morphology of solution-mined energy storage cavities, through dissolution experiments using brine and seawater in halite. *Q. J. Eng. Geol. Hydrogeol.* **2019**, *52*, 240–254.
- (43) Stiller, M.; Yechieli, Y.; Gavrieli, I. Rates of halite dissolution in natural brines: Dead Sea solutions as a case study. *Chem. Geol.* **2016**, *447*, 161–172.
- (44) Weisbrod, N.; Alon-Mordish, C.; Konen, E.; Yechieli, Y. Dynamic dissolution of halite rock during flow of diluted saline solutions. *Geophys. Res. Lett.* **2012**, *39*, L09404.
- (45) Alkattan, M.; Oelkers, E. H.; Dandurand, J.-L.; Schott, J. Experimental studies of halite dissolution kinetics, I The effect of saturation state and the presence of trace metals. *Chem. Geol.* **1997**, *137*, 201–219.
- (46) Simon, B. Dissolution rates of NaCl and KCl in aqueous solution. *J. Cryst. Growth* **1981**, *52*, 789–794.
- (47) Wagner, C. The Dissolution Rate of Sodium Chloride with Diffusion and Natural Convection as Rate-Determining Factors. *J. Phys. Colloid Chem.* **1949**, *53*, 1030–1033.
- (48) Dijk, P. E.; Berkowitz, B.; Yechieli, Y. Measurement and analysis of dissolution patterns in rock fractures. *Water Resour. Res.* **2002**, *38*, 5–1–5–12.
- (49) Alkattan, M.; Oelkers, E. H.; Dandurand, J.; Schott, J. Experimental studies of halite dissolution kinetics: II. The effect of the presence of aqueous trace anions and K₃Fe(CN)₆. *Chem. Geol.* **1997**, *143*, 17–26.
- (50) Harvie, C. E.; Møller, N.; Weare, J. H. The prediction of mineral solubilities in natural waters: The Na-K-Mg-Ca-H-Cl-SO₄-OH-HCO₃-CO₃-CO₂-H₂O system to high ionic strengths at 25°C. *Geochim. Cosmochim. Acta* **1984**, *48*, 723–751.
- (51) Parkhurst, D.; Appelo, T.; Parkhurst, D. L.; Appelo, C. A. J. Description of input and examples for PHREEQC version 3—a computer program for speciation, batch-reaction, one-dimensional transport, and inverse geochemical calculations. *US Geological Survey Techniques and Methods*; U.S. Geological Survey, 2013, Book 6, Chapter A43, p 497. Available only at <http://pubs.usgs.gov/tm/06/a43/>.
- (52) Pitzer, K. S. Thermodynamics of electrolytes. I. Theoretical basis and general equations. *J. Phys. Chem.* **1973**, *77*, 268–277.
- (53) Plummer, N.; Parkhurst, D. L.; Fleming, G. W.; Dunkle, S. A. *A Computer Program Incorporating Pitzer's Equations for Calculation of Geochemical Reactions in Brines*; Department of the Interior, US Geological Survey, 1988; pp 88–4153.
- (54) Yechieli, Y. Fresh-Saline Ground Water Interface in the Western Dead Sea Area. *Groundwater* **2000**, *38*, 615–623.
- (55) Gawad, S.; Schild, L.; Renaud, P. Micromachined impedance spectroscopy flow cytometer for cell analysis and particle sizing. *Lab Chip* **2001**, *1*, 76–82.

(56) Foutch, G. L.; Johannes, A. H. Reactors in Process Engineering. In *Encyclopedia of Physical Science and Technology*; Meyers, R. A., Ed., 3rd ed.; Academic Press: New York, 2003, pp 23–43.